JGR Solid Earth

RESEARCH ARTICLE
10.1029/2024JB029240

Modeling Subduction With Extremely Fast Trench Retreat

Diandian Peng[1] and **Dave Stegman**[1]

[1]Institute of Geophysics and Planetary Physics, Scripps Institution of Oceanography, University of California, San Diego, La Jolla, CA, USA

Key Points:

- Numerical models successfully replicate the unique geometry of the Tonga slab, including its kink and stagnation behavior
- Hybrid velocity boundary conditions and nonlinear rheology are essential for accurately modeling slabs undergoing rapid trench retreat
- The results resolve the paradox of the Tonga slab maintaining a steep dip angle despite experiencing the fastest known trench retreat

Correspondence to:

D. Peng,
d3peng@ucsd.edu

Citation:

Peng, D., & Stegman, D. (2024). Modeling subduction with extremely fast trench retreat. *Journal of Geophysical Research: Solid Earth*, *129*, e2024JB029240. https://doi.org/10.1029/2024JB029240

Received 4 APR 2024
Accepted 12 SEP 2024

Author Contributions:

Conceptualization: Diandian Peng, Dave Stegman
Data curation: Diandian Peng
Formal analysis: Diandian Peng
Funding acquisition: Dave Stegman
Investigation: Diandian Peng
Methodology: Diandian Peng, Dave Stegman
Project administration: Dave Stegman
Resources: Diandian Peng, Dave Stegman
Software: Diandian Peng
Supervision: Dave Stegman
Validation: Diandian Peng, Dave Stegman
Visualization: Diandian Peng
Writing – original draft: Diandian Peng
Writing – review & editing: Diandian Peng, Dave Stegman

Abstract The Tonga-Kermadec subduction zone exhibits the fastest observed trench retreat and convergence near its northern end. However, a paradox exists: despite the rapid trench retreat, the Tonga slab maintains a relatively steep dip angle above 400 km depth. The slab turns flat around 400 km, then steepening again until encountering a stagnant segment near 670 km. Despite its significance for understanding slab dynamics, no existing numerical model has successfully demonstrated how such a distinct slab morphology can be generated under the fast convergence. Here we run subduction models that successfully reproduce the slab geometries while incorporating the observed subduction rate. We use a hybrid velocity boundary condition, imposing velocities on the arc and subducting plate while allowing the overriding plate to respond freely. This approach is crucial for achieving a good match between the modeled and observed Tonga slab. The results explain how the detailed slab structure is highly sensitive to physical parameters including the seafloor age and the mantle viscosity. Notably, a nonlinear rheology, where dislocation creep reduces upper mantle viscosity under strong mantle flow, is essential. The weakened upper mantle allows for a faster slab sinking rate, which explains the large dip angle. Our findings highlight the utilizing rheological parameters that lead to extreme viscosity variations within numerical models to achieve an accurate representation of complex subduction systems like the Tonga-Kermadec zone. Our study opens new avenues for further study of ocean-ocean subduction systems, advancing our understanding of their role in shaping regional and global tectonics.

Plain Language Summary Tonga subduction zone is special in several ways. First, it has the fastest retreating trench. The maximum convergence rate is about 23 cm/yr, which is also the fastest worldwide. Second, images created using data from seismology indicate that a 1,000 km-long section of the subducted tectonic plate rests horizontally atop the 670 km discontinuity. Third, the same images show the upper mantle slab is kinked near 400 km depth. None of the previous mantle convection models can reproduce the Tonga slab structure when prescribed by the available histories of past plate motion. To overcome the difficulties of simulating this subduction zone, we developed numerical models with different types of boundary conditions and found it necessary to impose the velocity on the arc and subducting plate, while keep the overriding plate free slip. The distinct slab morphology is shaped by the mantle flow which strongly depends on the trench retreat rate, the mantle viscosity, and the seafloor age. In conclusion, our study underscores the importance of systematic evaluation of non-linear forward models for achieving a faithful representation of complex subduction systems like the Tonga-Kermadec zone.

1. Introduction

The trench of most subduction zones is retreating (Schellart et al., 2007). The retreat rate varies at different subduction zones, with the maximum value being ~16 cm/yr near the northern end of the Tonga subduction zone (Bevis et al., 1995; Schellart et al., 2007, 2008). As an important component of subduction, trench retreat is widely studied. It is proposed as controlling factor for the slab geometry and the opening of back-arc basin (Artemieva, 2023; Christensen, 1996; Goes et al., 2017; Heuret & Lallemand, 2005; Peng & Liu, 2023). The present-day trench migration rate decreases from north to south along this subduction zone (Figure 1). It is close to zero at the southern end of the Kermadec trench. The velocity of the Pacific Plate motion near the Tonga-Kermadec subduction zone is around 7 cm/yr. This leads to a 23 cm/yr maximum convergence, making it the fastest subduction zone. The reason for the superfast trench retreat and subduction is unclear. Possible mechanisms include fast mantle flow induced by slab avalanche (Pysklywec et al., 2003) and block rotation due to collision between the trench and the buoyant Louisville Seamount chain (Wallace et al., 2005).

Besides the fast trench retreat, the Tonga subduction zone is also well known for the stagnant slabs near the 670-km discontinuity (Amaru, 2007; Obayashi et al., 2013). However, there are large disagreements in different

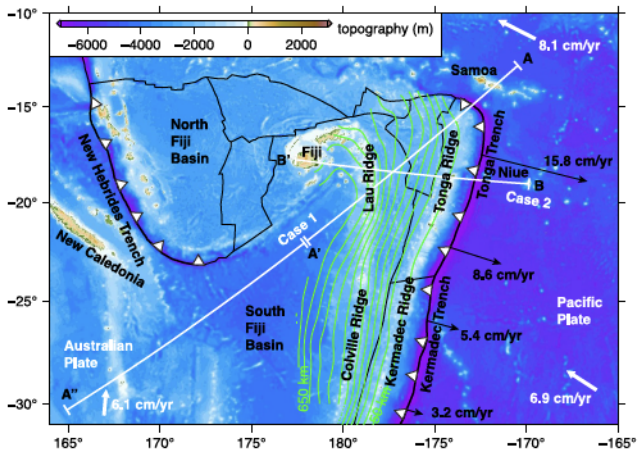

Figure 1. Map of the study region. The black arrows show the retreat rate along the Tonga-Kermadec trench (Schellart et al., 2007). The white arrows show the plate motion velocity (Schellart et al., 2007). The green contours mark the slab depth from slab2 (Hayes et al., 2018). The white lines show the cross-sections that we will discuss later. AA'A" (modeled with Case 1) is perpendicular to the trench. BB' (modeled with Case 2) is the same cross-section as in Conder and Wiens (2006). At the northern end of the Tonga-Kermadec trench, the trench retreat rate is the maximum worldwide, which leads to a convergence rate of about 23 cm/yr.

tomography studies. The stagnation of the Tonga slab is usually attributed to the fast trench retreat (Goes et al., 2017). In the upper mantle, the Tonga slab geometry varies with depth. Multiple studies based on seismic tomography and earthquake epicenters show that the Tonga slab has a kink around 400 km deep (Chen & Brudzinski, 2001; Conder & Wiens, 2006; Richards et al., 2011). The formation of the slab kink is a subject of debate. Previous studies have suggested that there may be another slab segment which either contributes to some of the anomalously distributed earthquakes (Chen & Brudzinski, 2001), collided with the Tonga slab (Richards et al., 2011) or bent the slab (Liu et al., 2021).

Because of its complexity and peculiarity, the Tonga-Kermadec subduction zone has been studied with lots of numerical models (Billen et al., 2003; Conder & Wiens, 2007; Liu et al., 2021; Pokorný et al., 2023). However, the distinct slab geometry under the extremely fast convergence rate is a first order problem that previous studies have been unable to fully address. Fast trench retreat rate has been proposed as a mechanism for the formation of flat slab that lies underneath the overriding plate (Espurt et al., 2008; Liu & Currie, 2016; Schellart & Strak, 2021). However, the dip of Tonga slab is about 53° (Syracuse et al., 2010), which is a large dip angle. We noticed one geodynamic study that created a naturally dipping slabs with a trench retreat rate close to that observed near Tonga (Leng & Gurnis, 2015), but since the modeled Pacific Plate is attached to the boundary and not moving toward the trench, the convergence rate is significantly underestimated. Currently, there is no numerical model that can reproduce the Tonga slab geometry while applying the trench retreat rate and subduction rate close to observed values (Figure 1). In addition, modeling subduction with an oceanic upper plate is still a challenging problem, making the Tonga subduction with its fast trench retreat an important natural archetype.

In this study, we ran two-dimensional (2D) mantle convection models to study the subduction of the Tonga slab. We used the observed slab structure as a constraint for numerical models with different types of velocity boundary conditions on the surface. We also investigated the trench retreat rate, rheology law, the background viscosity, seafloor age and phase transition at the 670 km discontinuity to understand their influence on the slab morphology.

2. Method

2.1. Governing Equations

In this study we model the subduction of Tonga slab in a two-dimensional equatorial slice of a sphere using the open source finite element code CitcomS (McNamara & Zhong, 2004; Tan & Gurnis, 2007; Zhong et al., 2000) with a Boussinesq approximation. The equations for the conservation of mass, momentum and energy and the advection of chemical tracers are:

$$\nabla \cdot \vec{u} = 0, \tag{1}$$

$$-\nabla P + \nabla \cdot \left[\eta\left(\nabla \vec{u} + \nabla^T \vec{u}\right)\right] + \left(\rho_m \alpha \Delta T + \Delta\rho_{ph}\Gamma + \Delta\rho_c C\right)\vec{g} = 0, \tag{2}$$

$$\frac{\partial T}{\partial t} + \vec{u} \cdot \nabla T = \kappa \nabla^2 T, \tag{3}$$

$$\frac{\partial C}{\partial t} + \vec{u} \cdot \nabla C = 0, \tag{4}$$

where $\vec{u}$ is the mantle flow velocity, P is the dynamic pressure, η is the dynamic viscosity, ρ_m is the density of the ambient mantle, α is the thermal expansion coefficient, κ is the thermal diffusivity, ΔT is the temperature

Table 1
List of Model Parameters

General parameters			Rheology parameters		
Symbol	Description	Value	Description	Diff.	Disl.
α	Thermal expansivity	3×10^{-5}1/K	Stress exponent *(n)*	1	3.5
κ	Thermal diffusivity	10^{-6} m^2/s	Activation energy in the upper mantle *(E)*	317 kJ/mol	496 kJ/mol
η_0	Reference viscosity	1×10^{21} Pas	Activation energy in the lower mantle *(E)*	317 kJ/mol	-
ρ_m	Reference density	3,340 kg/m^3	Activation volume in the upper mantle *(V)*	1.6e−6 m^3/mol	4.4e−6 m^3/mol
T_0	Reference temperature	1,400°C	Activation volume in the lower mantle *(V)*	6e−7 m^3/mol	-
R_0	Earth radius	6,371 km	Viscosity pre-factor in the upper mantle *(F)*	1.56e−11	1.15e−2
Ra	Rayleigh number	3.559×10^8	Viscosity pre-factor in the lower mantle *(F)*	3.0e−10	-

anomaly, $\Delta\rho_{ph}$ is the density jump across a phase change, Γ is the phase function, $\Delta\rho_c$ is the compositional density anomaly, C is composition and $\vec{g}$ is the gravitational acceleration. The model parameters are listed on Table 1.

2.2. Model Setup

The model domain extends from the surface to the core-mantle boundary (CMB), with a 2,876 km depth (Figure 2a). The horizontal span is 120°, which is about 13,343 km. We designed such a large horizontal model domain to minimize the effects of side boundaries on the model results. Each model has 1,025 nodes on the horizontal direction, and 225 nodes on the vertical direction. An uneven mesh is used which leads to a resolution of about 10 km on the horizontal direction. The vertical resolution is 6 km near the surface and 12 km near the CMB.

To investigate the effects of trench retreat and Pacific Plate motion on the slab evolution, we incorporate trench migration into the models. To implement this function, we employ a data-assimilation method that defines the surface velocity and lithospheric structure at each step (Liu & Stegman, 2011; Peng et al., 2021). We monitor the trench location based on the specified retreat rate. The Pacific Plate is defined on the eastern side of the trench, and the overriding plate is on the western side (Figure 2b). The overriding plate contains two parts, the Australian plate, and the *Arc*. In this paper, we used *Arc* to represent the part of the overriding plate which extends from the Tonga Ridge (volcanic arc) to the Tonga Trench. In Case 1, the width of the Arc is defined to be around 300 km. We defined the temperature profile and surface velocity individually for each of the Pacific Plate, Australian Plate, and the Arc.

2.3. Boundary and Initial Conditions

On the surface, both temperature and velocity boundaries are defined differently in the three different regions (Figure 2b), as illustrated below. In the models, the temperature at the bottom of lithosphere as well as model domain bottom is fixed at 1400°C. On the two sides, zero heat flux boundary is applied. The model has a fixed temperature on the surface everywhere except for the Arc. The Arc has an insulating boundary condition to permit free evolution. For the subducting Pacific Plate, the initial temperature profile is defined by the seafloor age following a plate model which is modified from a half-spacing cooling model (*i.e.*, seafloor older than 80 My is the same as 80 My). The temperature profile of the Pacific Plate is redefined at each step following the modified half-space cooling model. On the Australian Plate, we defined an initial linear temperature profile over a 120-km thick lithosphere. For the Arc, the initial temperature increases linearly with depth over an 80-km thick lithosphere (Figure 2b).

For velocity, the bottom and two sides are free slip. We define the extent of the Pacific Plate and the overriding plate on the surface based on the known trench location. The Pacific Plate has a westward velocity of 7 cm/yr imposed on the surface, consistent with the observed plate motion (Figure 1). On the overriding plate we adopt multiple ways to define the velocity boundary condition (VBC). In Type I VBC, the surface has a hybrid boundary condition comprised of an imposed velocity on the Arc and free slip on the Australian Plate. The imposed Arc velocity represents the intended trench retreat rate, enabling us to accurately model the trench retreat process. In

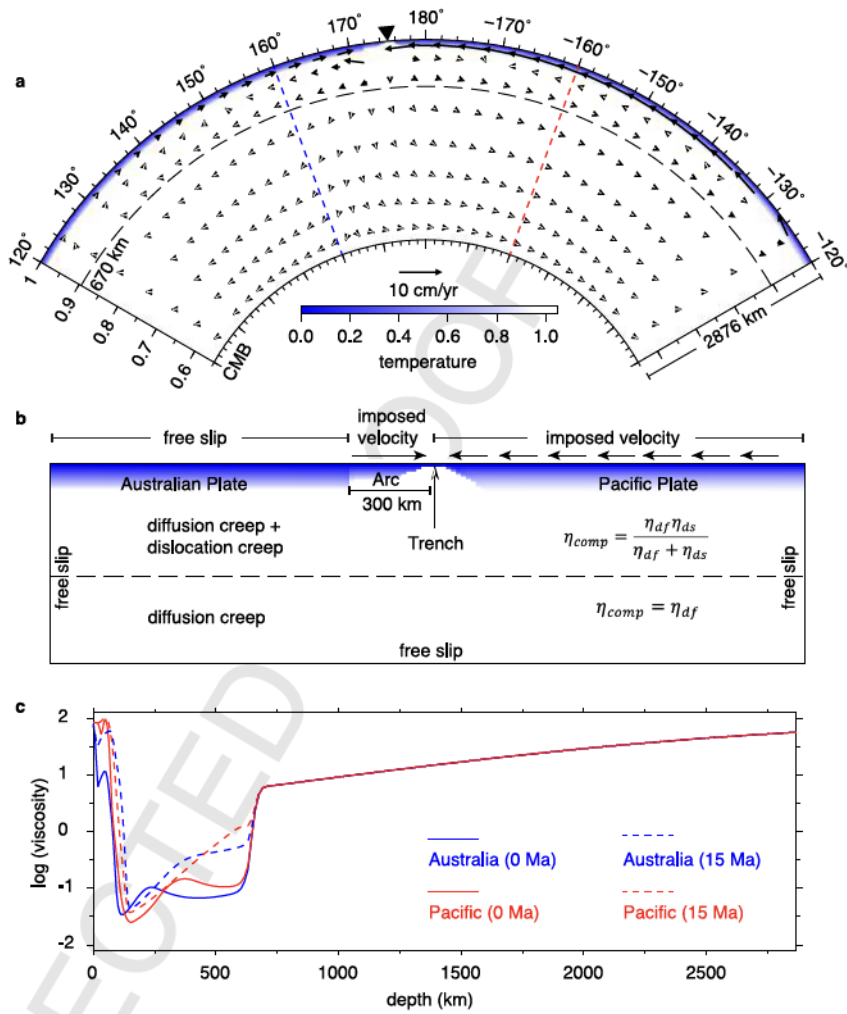

Figure 2. Model setup. (a) The model domain is 120° on the horizontal direction and 2,867 km on the vertical direction. The temperature and velocity field of the initial condition in Case 1 is shown. The black triangle shows the trench location. (b) Sketch (not to scale) of the boundary conditions with an emphasis near the trench. Surface velocity is imposed on the Pacific Plate and the Arc, while the Australian Plate is free slip in Case 1. (c) The radial viscosity profile beneath the Australian Plate and Pacific Plate (locations indicated by the blue and red dashed lines in a) at 15 Ma and 0 Ma.

Type II VBC, both the Australian Plate and the Arc have an imposed velocity identical to the trench retreat rate. In Type III VBC, both the Australian Plate and Arc are free slip.

2.4. Rheology Law

In the models we used a visco-plastic rheology (Arredondo & Billen, 2017; Billen & Hirth, 2007) (Figure 2c). The deformation parameters of olivine are based on laboratory values (Hirth & Kohlstedt, 2003). We only considered diffusion creep in the lower mantle. In the upper mantle, the deformation is composed of diffusion creep and dislocation creep. The composite viscosity of the upper mantle is the harmonic average of both parts.

$$\eta_{comp} = \frac{\eta_{df}\eta_{ds}}{\eta_{df}+\eta_{ds}}. \tag{5}$$

The viscosity law for each creep mechanism is

$$\eta_{df,ds} = F\dot{\varepsilon}_{II}^{(1-n)/n}\exp\left(\frac{E+PV}{nRT}\right), \tag{6}$$

where F is the pre-factor for different mechanisms and layers. $\dot{\varepsilon}_{II}$ is the second invariant of the strain rate tensor. For diffusion creep, n is 1. For dislocation creep, n is 3.5. E is the activation energy. V is the activation volume. P is the pressure. R is the gas constant. T is the temperature. The temperature profile in our models does not have an adiabatic increase with depth because of the Boussinesq approximation. To complement the lower value of temperature in Equation 6, we decrease the values of activation volume to 40% of laboratory values (Hirth & Kohlstedt, 2003). The background viscosity of the lowermost mantle increases by around 30-fold when $\dot{\varepsilon}_{II} = 1 \times 10^{-15}\ s^{-1}$. As the model evolves, the large strain rate induced by the fast mantle flow reduces the viscosity in the upper mantle (Figure 2c). The rheology parameters are provided in Table 1.

A yield stress is applied for low temperature lithosphere and slab,

$$\sigma_y = \min\left(\sigma_0 + \sigma_b(1-z), \sigma_{max}\right). \tag{7}$$

The yield stress on the surface is $\sigma_0 = 0.1$ MPa and increases with depth according to the gradient, $\sigma_b = 15$ MPa/km, up to a maximum yield stress of $\sigma_{max} = 500$ MPa, following Arredondo and Billen (2017). Because some or all the surface has an imposed velocity boundary condition, plasticity is not applied to the surface element in the models. The effective viscosity considering plasticity is

$$\eta_E = \min\left(\frac{\sigma_y}{\dot{\varepsilon}_{II}}, \eta_{comp}\right). \tag{8}$$

2.5. Composition

Chemical tracers are used to define different compositions with specific properties such as density and viscosity factor. A density of 2,800 kg/m³ is assigned to the 38 km-thick crustal tracers in the Australian Plate and the Arc. The tracers of the Australian Plate's lithospheric mantle have zero net chemical buoyancy. In contrast, the Arc has slightly lighter lithospheric mantle which contributes to its stability under conditions of strong mantle flow. Oceanic crustal tracers are assigned a density of 3,000 kg/m³, reflecting basaltic composition. During simulations, they transit to denser tracers when the depth exceeds 120 km, representing the basalt-to-eclogite phase transformation. Additionally, the tracers define a stronger lithosphere for the Arc compared to the Australian Plate. It is important to note that this effect is less significant than the viscosity variations induced by temperature dependence, strain rate, and plasticity.

3. Results

To investigate the sensitivity of the evolution and geometry of the Tonga slab to model parameters, we conducted 21 simulations. The models started from 15 Ma because the Lau Ridge was volcanically active 14–2 Ma (Artemieva, 2023). These models systematically tested variations in the velocity boundary conditions (Type I, II and III), the trench retreat rate, the Pacific Plate velocity, the width of the Arc, the rheological description, the seafloor age and the 670 km phase transition.

3.1. Slab Geometry

The Tonga-Kermadec subduction zone's ocean-to-ocean nature makes achieving a reliable seismic tomography model more challenging than in ocean-to-continent subduction zones. There are significant disagreements about the structure of the Tonga slab in tomography models (Goes et al., 2017). Several tomography models reveal stagnant slabs beneath Tonga and slabs penetrating the lower mantle beneath Kermadec, including GAP-P4 (Obayashi et al., 2013), UU-P07 (Amaru, 2007) and TX2019 (Lu et al., 2019). It is debated whether the stagnant Tonga slab is near 670 km or 1,000 km. In the upper mantle, the Tonga slab exhibits a unique geometry near its northern end, with a kink revealed by studies utilizing both hypocenter distributions and tomography (Chen & Brudzinski, 2001; Conder & Wiens, 2006; Richards et al., 2011). The slab dip angle is near 50° within the upper 400 km, followed by a flattening around 400 km depth. It then increases again and formed a steep slab as the slab approaches the 670-km discontinuity. To explain the variation in the Tonga slab's dip angle within the upper mantle, previous studies have proposed the presence of an additional slab segment within the region (Chen & Brudzinski, 2001; Liu et al., 2021; Richards et al., 2011). However, these hypotheses require further validation through future observations.

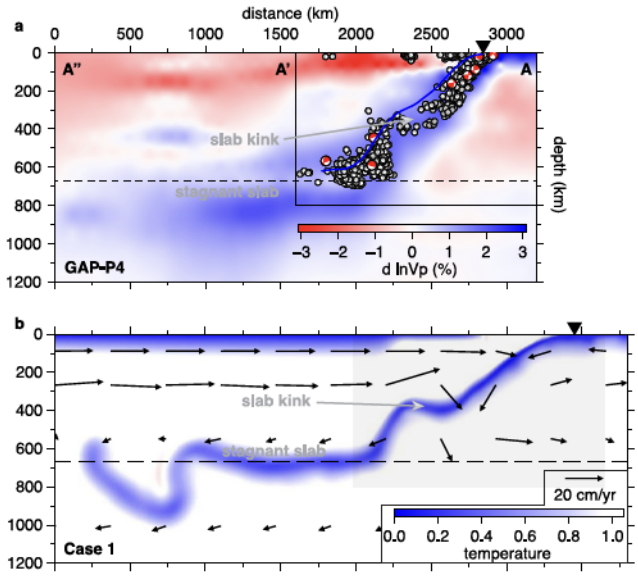

Figure 3. The comparison of observed slab geometry and model results along AA'A". (a) P wave anomalies in GAP-P4 tomography along AA'A". In the boxed region on the top right, the distribution of earthquake epicenters from the Global CMT catalog (beach balls) and the slab surface from the slab2 model (blue line) along AA' are plotted. (b) The temperature and velocity at the present-day in Case 1. The dashed line marks the 670 km discontinuity. The shaded region in (b) is aligned with the boxed region in (a).

In this study, we compared the slab geometry along two cross-sections that are perpendicular to the Tonga trench, AA'A" and BB' (Figure 1). We chose AA'A" because it only goes through one trench, which means the underneath Tonga slab is less affected by the New Hebrides/Vitiaz subduction. The tomographic image shows the stagnant Tonga slab clearly, but it is less defined whether it is stagnant near 670 km or 1,000 km (Figure 3a). For the detailed slab geometry in the upper mantle, we can refer to the distribution of epicenters (data collected from the Global CMT catalog) and the slab2 model (Hayes et al., 2018). We recognized the same pattern of slab dip angle variation with depth as in previous studies (Chen & Brudzinski, 2001; Richards et al., 2011). Two abrupt changes in the dip angle near 400 km led to a three-piece slab in the upper mantle. The nearly horizontally distributed epicenters of earthquakes mark the changes clearly.

From 400 to 600 km, it is a sub-vertical slab (Figure 3a). The same trend is shown by the slab2 model as well (Figure 3a). The slab kink is clear although the surface is smoothed in slab2. Using the geodynamic model with 16 cm/yr trench retreat rate (Case 1), we successfully reproduced the Tonga slab which qualitatively produces the observed slab structure (Figure 3). In the upper mantle, the slab dip angle variation matches observations almost perfectly. The modeled slab kink occurs near 400 km depth, featuring a 200 km-long flat segment. We propose that this specific feature is formed by the fast eastward mantle flow in the asthenosphere (above 400 km) induced by the rapidly subducting slab (see velocity arrows in Figure 3b). The Tonga slab is supported from beneath by the 670 km discontinuity due to the viscosity increase, phase transition, and other possible factors. Simultaneously, the fast asthenosphere pushes the shallow slab eastward. The contrasting mantle flow velocity above and below 400 km creates this unique feature.

Above 400 km, the calculated dip angle is slightly smaller than observed. From 400 to 670 km, the model's steeply dipping slab aligns well with the morphology indicated by the epicenters and slab2. Near the 670-km discontinuity, Case 1 reveals a 1000-km long stagnant slab, a feature consistent with findings from multiple tomography models, including GAP-P4 (Figure 3a), UU-P07 and TX2019. The oldest slab has subducted into the lower mantle and tilted into the mantle transition zone. This could contribute to the observed fast seismic anomalies in lower mantle tomography models.

The BB' cross-section is chosen to align with the high-resolution tomography study in Conder and Wiens (2006), for a direct comparison. Along BB', the slab exhibits a shallower dip angle above 400 km, which steepens below that depth (Figures 4a and 4b). Toward the 670 km discontinuity, a stagnant slab is formed (Figure 4b). To model the Tonga subduction along this cross-section, we applied a 12 cm/yr trench retreat rate. This aligns with the observed arc velocity (Figure 1), providing a realistic constraint on the surface velocity. This model (Case 2) also reproduced this dip angle variation with depth. The stagnant part of Tonga slab near 670 km is significantly longer in Case 1 than in Case 2 (Figures 3 and 4). The slab dip angle variation in the upper mantle is also different from that in Case 1. Along BB' there is no prominent flat segment of Tonga slab near 400 km, although there is still a sudden increase of dip angle (Figure 4c). These differences suggest that the trench retreat rate played an important role in the Tonga slab geometry.

3.2. Velocity Boundary Conditions

As previously described, we developed numerical models employing three types of velocity boundary conditions for the overriding plate. To evaluate the impact of these boundary conditions, we ran three models with varying trench retreat rates for each VBC type (Cases 1, 3–10 in Figure 5).

With a stationary Tonga trench during the past 15 Ma, the slab structure remains nearly identical across models using all three VBC types (not shown). Furthermore, when the retreat rate is 8 cm/yr or lower, the modeled slabs exhibit strong similarity regardless of VBC (Figures 5a–5c). This consistency demonstrates that the choice of VBC is not critical at low trench retreat rate, which is the condition addressed in most previous modeling studies.

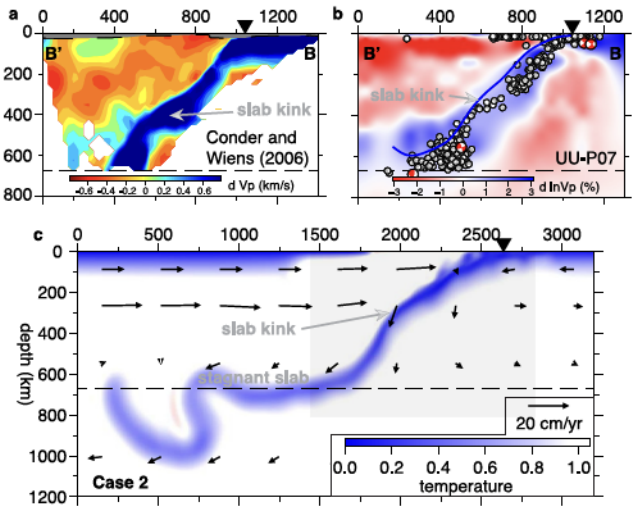

Figure 4. The comparison of observed slab geometry and model results along BB'. (a) P wave velocity anomalies from Conder and Wiens (2006). (b) The P wave velocity anomalies in UU-P07, the distribution of earthquake epicenters from the Global CMT catalog (beach balls) and the slab surface from the slab2 model (blue line). (c) The temperature and velocity at the present-day in Case 2. The dashed line marks the 670 km discontinuity. The shaded region in (c) is aligned with the figure domain in (a), (b).

As the trench retreat rate increases to 9 cm/yr and beyond, models utilizing Type III VBCs fail to generate realistic slab geometries (Figures 5f and i). The rapid retreat, which favors horizontal slab displacement coupled with the absence of mantle wedge flow, results in the slab adhering to the overriding plate. With even faster retreat rates, only Type I boundary conditions can replicate observed slab geometry (Figure 5g). While the earliest subducted slab in Case 9 descends into the mantle, the younger slab piled up in shallow mantle (Figure 5h). Its formation under fast trench retreat is consistent with previous studies (Liu & Currie, 2016; Schellart & Strak, 2021). Another noticeable problem with Type II VBC is that there is no back arc basin opening in all cases (Figures 5b–5h).

The behavior of Type II and Type III VBCs under varying retreat rates highlights the challenges of modeling subduction with super-fast trench retreat. Our results suggest that a hybrid velocity boundary condition on the overriding plate is essential for numerical models to investigate subduction zone dynamics with high trench retreat rates.

In addition, we also tested the influence of the Arc width (*i.e.*, the arc-trench gap) on the modeled slab structure. An early study suggested that the distance between volcanic arc and trench is 100–300 km globally, and lower than 200 km for Tonga subduction zone (Dickinson, 1973). A ~250 km arc-trench distance is presented in a recent study (Artemieva, 2023). In Case 1, the arc-trench gap is about 300 km. Considering the entire Tonga Ridge (instead of

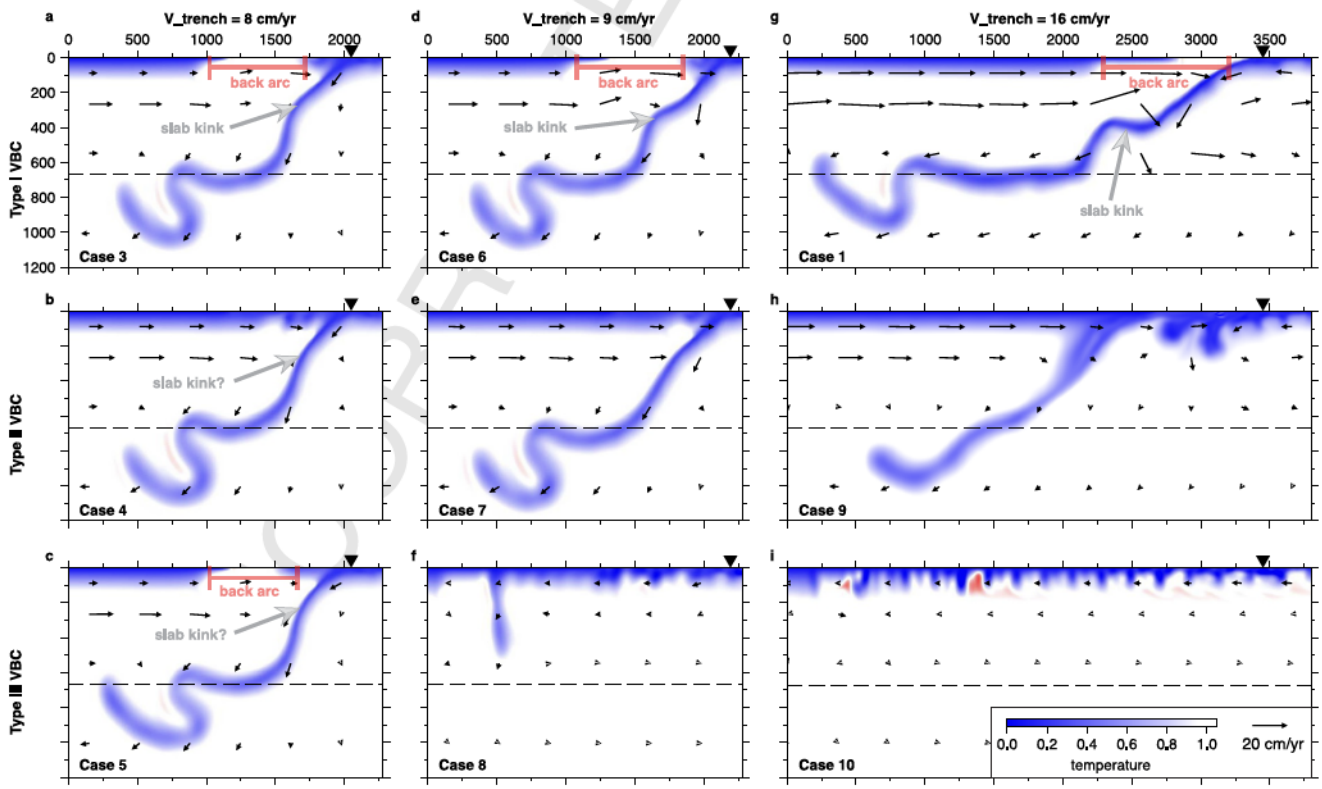

Figure 5. Models with three types of VBCs and different trench retreat rate. Upper row: Type I VBC. Middle row: Type II VBC. Lower row: Type III VBC. Left column: 8 cm/yr trench retreat rate. Middle column: 9 cm/yr trench retreat rate. Right column: 16 cm/yr trench retreat rate (a–c) When the Tonga trench rate is 8 cm/yr, the Tonga slab is similar in Cases 3–5 (d–f) When trench retreat rate is 9 cm/yr, Case 6 (d) and 7 (e) have similar slab structure, but Case 8 (f) stopped creating a natural slab because of the free slip VBC on the Australian Plate and the Arc (g–h) With super-fast trench retreat, only Case 1 (g) has the correct slab structure. Neither Case 9 (h) and Case 10 (i) can generate a Tonga slab like the observed. The red bars represent the back arc basin.

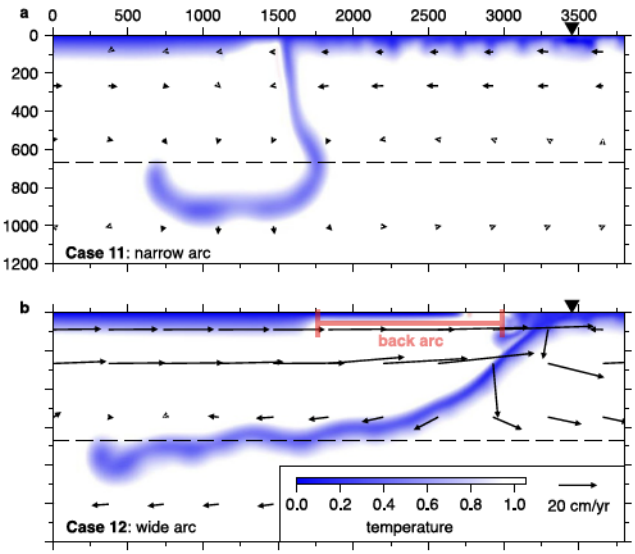

Figure 6. Impact of Arc width on slab geometry and mantle wedge dynamics. (a) Case 11: A narrow Arc (100 km) limits mantle flow within the wedge. (b) Case 12: A wide Arc (500 km) facilitates vigorous mantle flow, creating a prominent mantle wedge. Note: Cases 11 and 12 share identical parameters with Case 1, differing only in Arc width.

just the arc front) as part of the Arc region in the models, this value surpasses observed distances between the arc front and trench axis. To investigate the effects of the arc-trench distance width, we ran two additional models in which the Arc width is about 100 km (Case 11) and 500 km (Case 12), respectively (Figure 6).

A narrow Arc region (Case 11, Figure 6a) impedes the recent subduction from sinking into deep mantle. Conversely, an excessively wide Arc (Case 12, Figure 6b) produces a naturally dipping slab but fails to capture the observed slab kink (Figure 3a). Comparing Case 1 (Figure 5g) with Cases 11–12 (Figure 6), a wider Arc significantly enhances the mantle wedge flow. These results emphasize the importance of incorporating an arc-trench system geometry that closely resembles real-world observations when modeling the Tonga subduction zone using Type I boundary condition.

3.3. Mantle Viscosity

It has been shown that a low viscosity mantle wedge is important for the multiple aspect including back-arc spreading in the Tonga-Kermadec subduction zone and the fast mantle flow (Billen et al., 2003; Conder & Wiens, 2007). As the Tonga subduction zone has the largest convergence rate (Figure 1), we can expect a fast mantle flow around the slab. The upper mantle viscosity, which is decided by deformation composed of diffusion creep and dislocation (Hirth & Kohlstedt, 2003), should be low due to the large strain rate. In Case 1, the upper mantle has low viscosity due to the nonlinear rheology law applied (Figure 7a). For comparison, we also ran two tests (Cases 13–14) using linear rheology without dislocation creep, while maintaining plasticity (Figures 7b and 7c). The lower mantle strength in Cases 1 and 13–14 is consistent due to the same rheology law and parameters (Figures 7a–7c). In the upper mantle, Case 13 has the same rheology parameters as Case 1 but is significantly stronger because of the Newtonian rheology. In contrast, Case 14 has pre-factors (F in Equation 6) 0.1 times weaker than Case 1, achieving a comparably weak upper mantle without dislocation creep. In Case 13, the slab encountered strong viscous resistance and formed a folded structure in the shallow mantle (Figure 7b). In Case 14, a naturally dipping slab in the upper mantle and a stagnant segment near 670 km are created (Figure 7c). These tests demonstrate that for subduction zones with rapid trench retreat, the upper mantle needs to be extremely weak to produce a generally large dip angle. Nonlinear rheology is the most reasonable explanation for the weak upper mantle, as the fast mantle flow associated with rapid trench retreat increases the strain rate, contributing to the low viscosity through dislocation creep. Conversely, uniformly reduced pre-factors, as in Case 14, results in an unrealistically weak upper mantle globally. Therefore, nonlinear rheology is essential for accurately modeling the Tonga slab subduction.

Moreover, we also tested two different background viscosity profiles with nonlinear rheology by varying the pre-fectors. Case 15 has the same upper mantle viscosity as in Case 1 but has a weaker lower mantle (Figure 7d). We find that there is still a stagnant slab near the 670 km discontinuity. However, the upper mantle slab does not have the slab kink as in Case 1 (Figure 7a). In Case 16, both upper mantle and lower mantle is stronger (Figure 7e). Although the upper mantle has weakened areas, the overall viscosity is larger than Case 1 (Figure 7a). Eventually, a flat slab lying underneath the Australian Plate is created (Figure 7e). These tests show that the upper mantle slab dip angle variation is very sensitive to the physical properties of both upper mantle and lower mantle. Although the length and morphology of the stagnant slab differ in Cases 1 and 14–16, its existence suggests that its formation is less sensitive to the mantle viscosity profile than the 400 km slab kink.

3.4. Other Factors

Other factors influencing subduction dynamics include the seafloor age and the phase transition at the 670 km discontinuity. The present-day Pacific seafloor near the Tonga subduction zone is exceptionally old, exceeding 100 million years (My). Older seafloor translates to colder, denser oceanic lithosphere, resulting in a higher density subducted slab. Studies of the slab thermal parameters suggest that the Tonga slab is the coldest because of its old age and fast subduction (Syracuse et al., 2010; Van Keken et al., 2011).

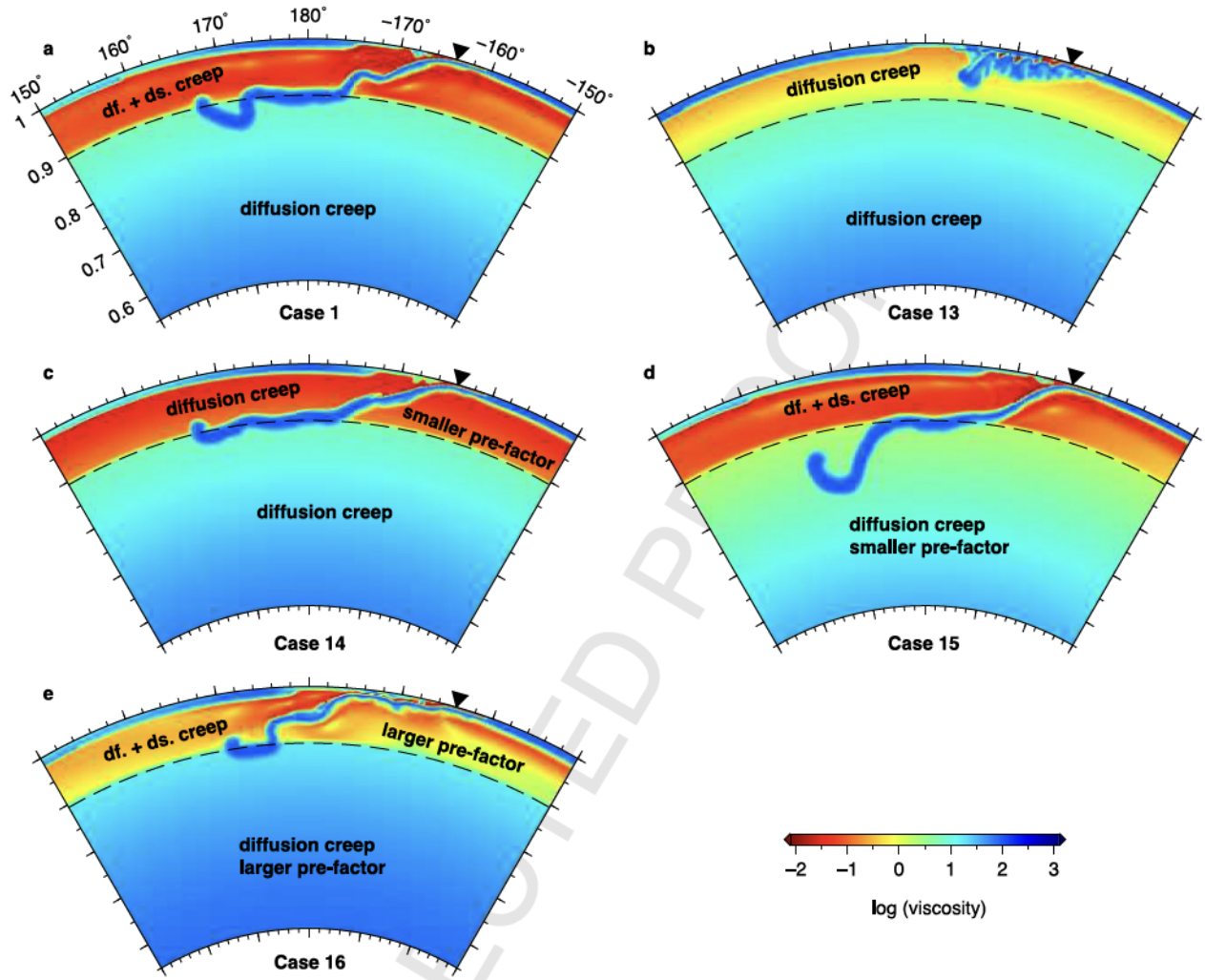

Figure 7. The effects of mantle viscosity on slab geometry (a–e) The present-day viscosity in Case 1 and Cases 13–16, respectively. Viscosity is presented on a logarithmic scale relative to the reference value (10^{21} Pas). The dashed line indicates the 670 km discontinuity.

To investigate the impact of seafloor age on slab geometry, we ran an additional model (Case 17) featuring a younger (30 My old) Pacific Plate. In this scenario, the subducted slab lacks sufficient negative buoyancy due to its younger age, hindering its descent (Figure 8a). Consequently, the recently subducted portion forms a flat and folded slab in shallow mantle. The contrasting outcomes between Case 17 and Case 1 (Figure 3b) highlight the important role of the Pacific Plate's age in accurately replicating the geometry of the Tonga slab.

The 670 km depth discontinuity, where a phase transition is known to occur in the mantle, is often considered a key factor in slab stagnation (Tackley et al., 1993). In the previously discussed models, we incorporated this phase transition with a Clapeyron slope of −2.0 MPa/K. To assess its influence in the Tonga slab, we conducted a simulation (Case 18) that excluded the phase transition.

Compared to Case 1 with the phase transition (Figure 3b), the Tonga slab in Case 18 exhibits some degree of bending at the 670 km depth (Figure 8b). While this suggests a less stagnant behavior compared to Case 1, the overall slab geometry remains relatively similar. This observation indicates that the phase transition plays a contributory role in creating a truly stagnant slab, but for the Tonga system, the fast trench retreat appears to be the dominant control factor on slab dynamics.

Furthermore, the presence of the slab kink around 400 km depth is reproduced in both simulations (Cases 1 and 18). This reinforces our earlier hypothesis that the rapid eastward asthenosphere flow is the primary driver for the formation of this specific feature, with the 670 km phase transition having a limited influence.

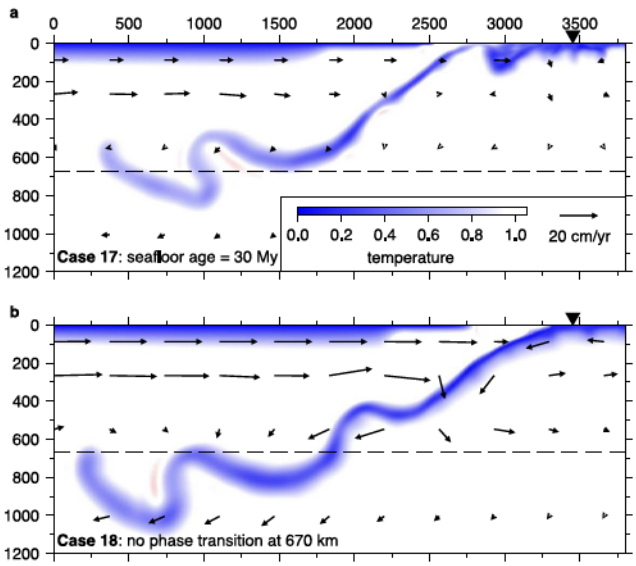

Figure 8. Modeled temperature and velocity field of Tonga slab with a younger Pacific Plate (a, Case 17) and without the 670 km phase transition (b, Case 18).

3.5. Reference Frame

A reference frame is necessary to describe the surface plate motion velocity. Under different reference frame, the plate motion and trench retreat rate vary significantly (Schellart et al., 2008), while the convergence rates at subduction zones remain unchanged. Schellart et al. (2008) found that the Indo-Atlantic hotspot reference frame is the best for calculating plate velocities and plate boundary velocities. Their calculation concluded a maximum 16 cm/yr trench retreat rate for the Tonga trench and about 7 cm/yr Pacific Plate velocity near the subduction zone (Figure 1).

A common assumption is that numerical models will produce reasonable results as long as the convergence rate is held constant while changing the velocity of the subducting plate. For example, some recent studies applied the convergence rate to the subducting plate while keeping the trench and overriding plate stationary to model the Tonga slab subduction (Palmiotto et al., 2022). To challenge this assumption, we ran three models with varying Pacific Plate velocities and trench retreat rates, maintaining a total convergence rate of 23 cm/yr (Figure 9). Our goal was to investigate the impact that different reference frames might have on model outcomes, even when convergence rate remains constant.

In Case 19, the trench is not migrating. The subducted Tonga slab piled and folded up beneath the trench (Figure 9a). Beneath the Pacific Plate, the shallow mantle flow is Couette-type flow which is controlled by the imposed surface velocity. Beneath the Australian Plate, the mantle flow is Poiseuille-type, which is induced by the sinking slab. The magnitudes of the mantle flow of the two sides of the slab are similar, thus the slab is almost vertical. When the trench retreat rate is 8 cm/yr (Case 20), an asymmetric slab formed (Figure 9b). In the upper mantle, the wedge has faster flow velocity than beneath the Pacific Plate. Case 1 has the trench retreat rate and Pacific Plate velocity as observed (Schellart et al., 2007). Eventually, the slab geometry mimics the observed Tonga slab (Figures 3 and 9c). When the trench retreat rate is increased to 23 cm/yr (Case 21), the overall slab dip angle is smaller, and the recently subducted slab cannot be decoupled from the overriding plate (Figure 9d). The differences in mantle flow and slab geometry among these models are significant. The mantle beneath the Tonga-Kermadec subduction zone should have limited background velocity (Peng & Liu, 2023). We conclude that selecting a reasonable reference frame is crucial for the accuracy and reliability of numerical mantle convection models. In addition, stagnant slabs near the 670-km discontinuity in Cases 1 and 21, but not in Cases 19–20. This further confirms that the fast trench retreat is an important reason for the slab stagnation near the 670 km discontinuity.

4. Discussion

4.1. The Fast Convergence Subduction Rate

A fast trench retreat rate has been linked to the formation of flat slabs in subduction zones plate (Espurt et al., 2008; Liu & Currie, 2016; Schellart & Strak, 2021). However, the Tonga subduction zone exhibits a paradox: despite having the fastest observed trench retreat rate, the Tonga slab maintains a relatively steep dip angle of around 50° (Figures 3 and 4). Existing models fail to explain this discrepancy.

While a fast retreat rate promotes horizontal slab movement, a significant vertical sinking velocity is necessary for a large dip angle. Studies suggest the Tonga slab is exceptionally cold due to its old age and rapid subduction (Syracuse et al., 2010; Van Keken et al., 2011). Cold slabs are denser, which enhances the sinking rate. Our modeling results support the importance of the Pacific Plate's old age (Figure 8a). However, the Izu-Bonin-Mariana subduction zone has an even older Pacific Plate yet exhibits a slower sinking rate. Therefore, old seafloor alone is not the deciding factor of fast slab sinking.

Based on our model results, we propose that the reduced resistance to slab sinking by the non-linear weakening of the upper mantle is the major reason for the fast sinking of Tonga slab. On the one hand, the fastest trench retreat and convergence rate is observed (Figure 1). On the other hand, it is widely accepted that the upper mantle olivine deformation is controlled by both diffusion and dislocation creep (Hirth & Kohlstedt, 2003; Karato & Wu, 1993).

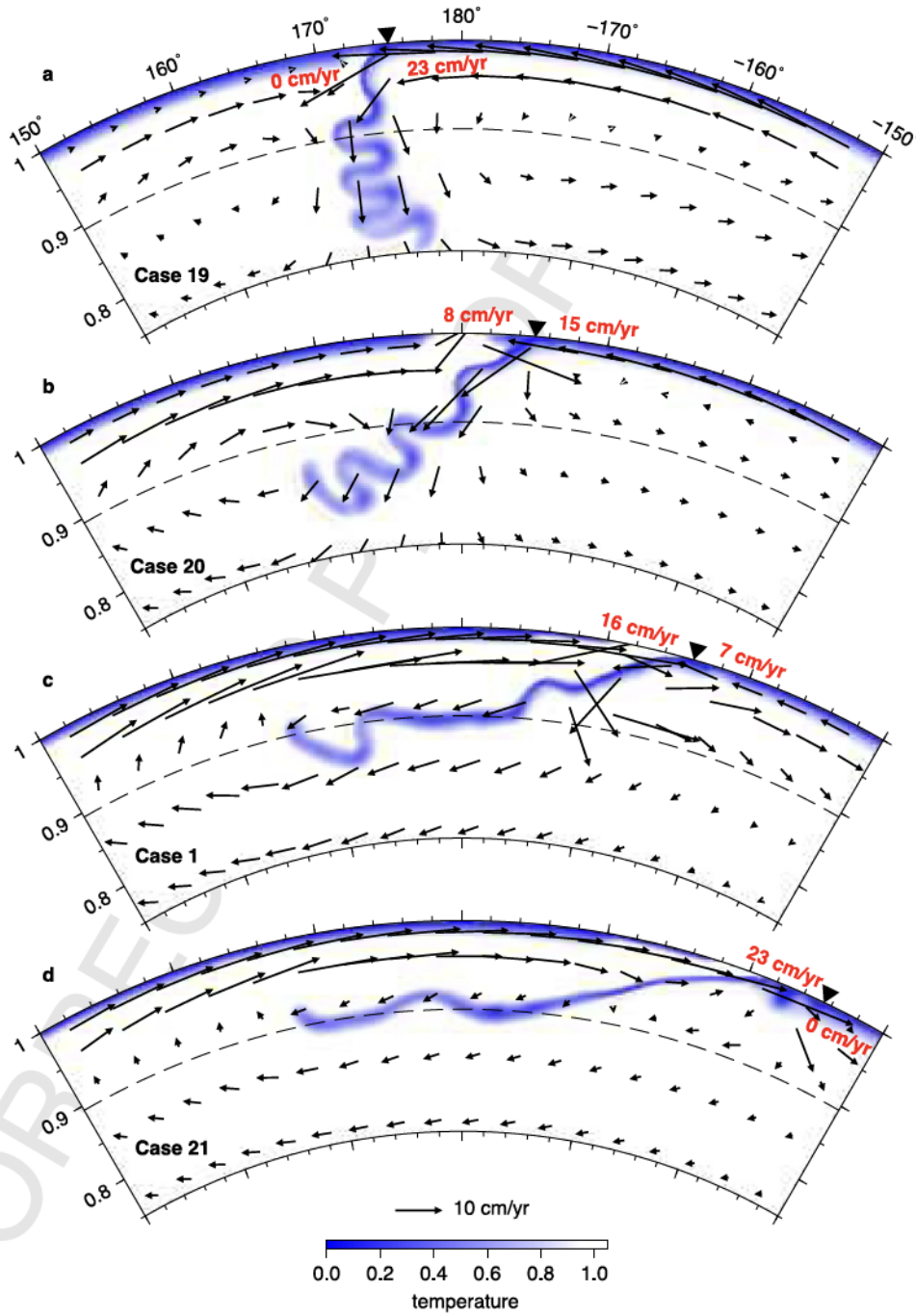

Figure 9. Effects of trench retreat rate on slab geometry with a constant 23 cm/yr convergence rate. (a) Case 19: Stationary trench, Pacific Plate velocity of 23 cm/yr. (b) Case 20: Trench retreat rate of 8 cm/yr, Pacific Plate velocity of 15 cm/yr. (c) Case 1: Trench retreat rate of 16 cm/yr, Pacific Plate velocity of 7 cm/yr. (d) Case 21: Trench retreat rate of 23 cm/yr, stationary Pacific Plate. Dashed line indicates the 670 km discontinuity.

The fast mantle flow is expected to increase the strain rate and thus decrease the mantle viscosity, as it is in the models (Figure 7). A weaker upper mantle leads to smaller resistant force and faster sinking rates. As a result, the Tonga slab has a large dip angle while the trench retreat rate is large. The low-viscosity mantle wedge is also proposed by previous studies (Billen et al., 2003; Billen & Gurnis, 2001; Conder & Wiens, 2007), consistent with our results, is also important to maintain viscous decoupling between the slab and the upper plate.

4.2. The Special Slab Geometry

The stagnant slab segment near the 670-km discontinuity beneath the Tonga subduction zone is a topic of many studies, with a fast trench retreat rate being the prevailing explanation for its formation (Christensen, 1996; Goes et al., 2017; Peng & Liu, 2023). Our modeling results support this hypothesis (Figure 9).

However, the origin of the slab kink observed around 400 km depth remains a subject of debate. Previous studies have attributed this feature to the interaction between the Tonga slab and another subducted slab (Chen & Brudzinski, 2001; Liu et al., 2021; Richards et al., 2011). In contrast, our findings suggest that this slab kink geometry can arise naturally due to the contrasting horizontal mantle flow velocity above and below 400 km, without the necessity of a separate slab (Figure 3). In addition, recent research also proposed that changes in the Tonga slab stress state can be explained by the subduction of a single slab (Pokorný et al., 2023), eliminating the need for a relic slab (Liu et al., 2021). To definitively assess the potential influence of the New Hebrides/Vitiaz subduction zone on the observed Tonga slab morphology, future studies incorporating numerical models with an additional subducted slab are warranted.

4.3. Types of Surface Velocity Boundary Conditions

Our testing of three distinct velocity boundary conditions revealed that Type I VBC yields the most accurate results for modeling the Tonga subduction zone. Furthermore, when the trench retreat rate remains below 8 cm/yr, all three VBC types produced remarkably similar outcomes (Figure 5). Recognizing that the majority of global subduction zones exhibit retreat rates lower than 8 cm/yr (Schellart et al., 2007), these results suggest that the specific choice of VBC may hold a limited influence on model behavior within this common range of trench motion.

Our models employ imposed velocities on the Pacific Plate, defining them as kinematic models driven by velocity boundary conditions. We opted for this approach, rather than fully dynamic models which are self-driven by the internal density anomalies, for several compelling reasons. First, we are able to leverage existing knowledge because the Cenozoic motion of the Pacific Plate is well-established, particularly with constraints from hotspot tracks like the Hawaii-Emperor and Louisville Seamount Chains. Kinematic models enable us to optimally incorporate the available plate motion data. Second, we chose to incorporate the motion of the plate boundary itself instead of the motion of the overriding plate. Since only the present-day trench retreat rates are known through observation, varying the imposed trench retreat rate allows us to test which scenarios best explain the observed slab morphology. This eliminates the need to reconcile model predictions with inferred trench migration rates from plate reconstructions which have uncertainty. Third, fully dynamic models face greater complexities when aiming to reproduce observed plate motions and mantle structures, so our hybrid models offer a step of forward progress toward overcoming those challenges. Matching recent plate motion histories and current velocities requires incorporating numerous factors, creating a significant modeling challenge (Hu et al., 2022; Stadler et al., 2010).

In contrast to the free-slip or imposed velocity boundary conditions utilized in our models, an alternative approach involves implementing a free surface or pseudo-free surface (Crameri et al., 2012a, 2012b; Schmeling et al., 2008). Free surface models have demonstrated advantages in favoring single-sided subduction and more accurately predicting topography. However, to fully utilize observational data such as plate motion and trench velocities, we have two primary options. First, imposing surface velocities (as employed in this study). This directly integrates known constraints but might limit the model's ability to self-determine surface expressions. Second, developing internal velocity boundary conditions. This would maintain a more dynamic character within the model but could increase complexity and introduce uncertainty into model outputs.

4.4. Limitations of 2D Models in Investigating Tonga Subduction

The 2D nature of the models employed in this study imposes inherent limitations when examining certain aspects of the Tonga subduction zone. Here are two key areas where 3D models would provide a more comprehensive analysis.

First, to study the Tonga slab geometry along AA'A" and BB', our models have different trench retreat rates with correspondence to the observed velocity on the Tonga arc (Figure 1). However, simulating subduction for cross-sections AA'A" and BB' (Figure 1) in isolated 2D models might not accurately represent their interaction within

the same subduction system. A single 3D model encompassing both cross-sections would likely yield different, and potentially more realistic, slab geometries compared to two separate 2D models.

Second, the rollback of the Tonga slab may induce a significant toroidal flow, with mantle moving from beneath the slab to the mantle wedge on a horizontal plane (Li et al., 2019; Stegman et al., 2006). This flow is thought to explain seismic anisotropy observations (Foley & Long, 2011; Long, 2013; Yu et al., 2022) and potential mixing of Samoan Plume signals into back-arc basins (Chang et al., 2016; Druken et al., 2014; Price et al., 2014). Investigating these phenomena is inherently impossible within the constraints of a 2D model.

5. Conclusion

This study successfully employed 2D mantle convection models to replicate two distinctive features of the Tonga subduction zone: the slab kink around 400 km depth and the stagnant slab near the 670-km discontinuity. Our findings underscore the challenges of modeling subduction zones characterized by exceptionally high convergence rates and rapid trench retreat. We determined that the Tonga slab morphology is highly sensitive to various model parameters in these extreme conditions.

Crucially, our results demonstrate that a hybrid velocity boundary condition (VBC) on the overriding plate is necessary to accurately simulate rapid trench retreat. Moreover, the width of the Arc region, where the trench retreat velocity is applied, should closely resemble observed values for optimal model performance.

Additionally, incorporating nonlinear rheology is essential as it allows for upper mantle weakening under high strain rates, contributing to a large slab dip angle while the trench retreat is extremely fast. The age of the Pacific Plate proved to be another key factor, directly influencing slab density and, consequently, the slab sinking rate and geometry. Finally, we established that changing the mantle reference frame significantly impacts surface velocities, potentially leading to inaccurate slab geometry representations.

These findings emphasize the importance of employing Earth-like parameters and configurations within numerical models to achieve a faithful representation of complex subduction systems like the Tonga-Kermadec zone. Our work provides valuable insights for future research aimed at modeling such geologically dynamic regions.

Data Availability Statement

The figures are plotted with GMT (https://www.generic-mapping-tools.org/). The finite element code CitcomS is available at https://geodynamics.org/resources/citcoms/ (Moresi et al., 2014). The P wave tomography model UU-P07 is available at https://www.atlas-of-the-underworld.org/uu-p07-model/. GAP-P4 is available at http://136.144.177.195/models/GAP-P4.tar.gz. The model input parameters and output files are available at Zenodo via DOI:10.5281/zenodo.12626942 (Peng, 2024).

Acknowledgments
The authors gratefully acknowledge support from the National Science Foundation (NSF) Award 1928970. D.P. extends thanks to the Green Foundation for their support. We acknowledge the HPC resources provided by the Frontera computing project at the Texas Advanced Computing Center (TACC) made possible by National Science Foundation award OAC-1818253. Additionally, we express our gratitude to Dave May for valuable discussions regarding nonlinear rheology.

References

Amaru, M. (2007). Global travel time tomography with 3-D reference models. *Geologica Ultraiectina*, *274*, 174.
Arredondo, K. M., & Billen, M. I. (2017). Coupled effects of phase transitions and rheology in 2-D dynamical models of subduction. *Journal of Geophysical Research: Solid Earth*, *122*(7), 5813–5830. https://doi.org/10.1002/2017JB014374
Artemieva, I. M. (2023). Back-arc basins: A global view from geophysical synthesis and analysis. *Earth-Science Reviews*, *236*, 104242. https://doi.org/10.1016/j.earscirev.2022.104242
Bevis, M., Taylor, F. W., Schutz, B. E., Recy, J., Isacks, B. L., Helu, S., et al. (1995). Geodetic observations of very rapid convergence and back-arc extension at the Tonga arc. *Nature*, *374*(6519), 249–251. https://doi.org/10.1038/374249a0
Billen, M. I., & Gurnis, M. (2001). A low viscosity wedge in subduction zones. *Earth and Planetary Science Letters*, *193*(1–2), 227–236. https://doi.org/10.1016/S0012-821X(01)00482-4
Billen, M. I., Gurnis, M., & Simons, M. (2003). Multiscale dynamics of the Tonga-Kermadec subduction zone. *Geophysical Journal International*, *153*(2), 359–388. https://doi.org/10.1046/j.1365-246X.2003.01915.x
Billen, M. I., & Hirth, G. (2007). Rheologic controls on slab dynamics. *Geochemistry, Geophysics, Geosystems*, *8*(8), 2007GC001597. https://doi.org/10.1029/2007GC001597
Chang, S.-J., Ferreira, A. M. G., & Faccenda, M. (2016). Upper- and mid-mantle interaction between the Samoan plume and the Tonga–Kermadec slabs. *Nature Communications*, *7*(1), 10799. https://doi.org/10.1038/ncomms10799
Chen, W.-P., & Brudzinski, M. R. (2001). Evidence for a large-scale remnant of subducted lithosphere beneath Fiji. *Science*, *292*(5526), 2475–2479. https://doi.org/10.1126/science.292.5526.2475
Christensen, U. R. (1996). The influence of trench migration on slab penetration into the lower mantle. *Earth and Planetary Science Letters*, *140*(1–4), 27–39. https://doi.org/10.1016/0012-821X(96)00023-4

Conder, J. A., & Wiens, D. A. (2006). Seismic structure beneath the Tonga arc and Lau back-arc basin determined from joint Vp, Vp/Vs tomography. *Geochemistry, Geophysics, Geosystems*, *7*(3), 2005GC001113. https://doi.org/10.1029/2005GC001113

Conder, J. A., & Wiens, D. A. (2007). Rapid mantle flow beneath the Tonga volcanic arc. *Earth and Planetary Science Letters*, *264*(1–2), 299–307. https://doi.org/10.1016/j.epsl.2007.10.014

Crameri, F., Schmeling, H., Golabek, G. J., Duretz, T., Orendt, R., Buiter, S. J. H., et al. (2012). A comparison of numerical surface topography calculations in geodynamic modelling: An evaluation of the 'sticky air' method: Modelling topography in geodynamics. *Geophysical Journal International*, *189*(1), 38–54. https://doi.org/10.1111/j.1365-246X.2012.05388.x

Crameri, F., Tackley, P. J., Meilick, I., Gerya, T. V., & Kaus, B. J. P. (2012). A free plate surface and weak oceanic crust produce single-sided subduction on Earth. *Geophysical Research Letters*, *39*(3), 2011GL050046. https://doi.org/10.1029/2011GL050046

Dickinson, W. R. (1973). Widths of modern arc-trench gaps proportional to past duration of igneous activity in associated magmatic arcs. *Journal of Geophysical Research*, *78*(17), 3376–3389. https://doi.org/10.1029/JB078i017p03376

Druken, K. A., Kincaid, C., Griffiths, R. W., Stegman, D. R., & Hart, S. R. (2014). Plume–slab interaction: The Samoa–Tonga system. *Physics of the Earth and Planetary Interiors*, *232*, 1–14. https://doi.org/10.1016/j.pepi.2014.03.003

Espurt, N., Funiciello, F., Martinod, J., Guillaume, B., Regard, V., Faccenna, C., & Brusset, S. (2008). Flat subduction dynamics and deformation of the South American plate: Insights from analog modeling. *Tectonics*, *27*(3), 2007TC002175. https://doi.org/10.1029/2007TC002175

Foley, B. J., & Long, M. D. (2011). Upper and mid-mantle anisotropy beneath the Tonga slab: Anisotropy beneath Tonga slab. *Geophysical Research Letters*, *38*(2), n/a-n–a. https://doi.org/10.1029/2010GL046021

Goes, S., Agrusta, R., Van Hunen, J., & Garel, F. (2017). Subduction-transition zone interaction: A review. *Geosphere*, *13*(3), 644–664. https://doi.org/10.1130/GES01476.1

Hayes, G. P., Moore, G. L., Portner, D. E., Hearne, M., Flamme, H., Furtney, M., & Smoczyk, G. M. (2018). Slab2, a comprehensive subduction zone geometry model. *Science*, *362*(6410), 58–61. https://doi.org/10.1126/science.aat4723

Heuret, A., & Lallemand, S. (2005). Plate motions, slab dynamics and back-arc deformation. *Physics of the Earth and Planetary Interiors*, *149*(1–2), 31–51. https://doi.org/10.1016/j.pepi.2004.08.022

Hirth, G., & Kohlstedt, D. (2003). Rheology of the upper mantle and the mantle wedge: A view from the experimentalists. In J. Eiler (Ed.), *Geophysical monograph series* (Vol. 138, pp. 83–105). American Geophysical Union. https://doi.org/10.1029/138GM06

Hu, J., Gurnis, M., Rudi, J., Stadler, G., & Müller, R. D. (2022). Dynamics of the abrupt change in Pacific Plate motion around 50 million years ago. *Nature Geoscience*, *15*(1), 74–78. https://doi.org/10.1038/s41561-021-00862-6

Karato, S., & Wu, P. (1993). Rheology of the upper mantle: A synthesis. *Science*, *260*(5109), 771–778. https://doi.org/10.1126/science.260.5109.771

Leng, W., & Gurnis, M. (2015). Subduction initiation at relic arcs. *Geophysical Research Letters*, *42*(17), 7014–7021. https://doi.org/10.1002/2015GL064985

Li, L., Chen, Y., Zheng, Y., Hu, H., & Wu, J. (2019). Seismic evidence for plume-slab interaction by high-resolution imaging of the 410-km discontinuity under Tonga. *Geophysical Research Letters*, *46*(23), 13687–13694. https://doi.org/10.1029/2019GL084164

Liu, H., Gurnis, M., Leng, W., Jia, Z., & Zhan, Z. (2021). Tonga slab morphology and stress variations controlled by a relic slab: Implications for deep earthquakes in the Tonga-Fiji region. *Geophysical Research Letters*, *48*(7), e2020GL091331. https://doi.org/10.1029/2020GL091331

Liu, L., & Stegman, D. R. (2011). Segmentation of the Farallon slab. *Earth and Planetary Science Letters*, *311*(1–2), 1–10. https://doi.org/10.1016/j.epsl.2011.09.027

Liu, S., & Currie, C. A. (2016). Farallon plate dynamics prior to the Laramide orogeny: Numerical models of flat subduction. *Tectonophysics*, *666*, 33–47. https://doi.org/10.1016/j.tecto.2015.10.010

Long, M. D. (2013). Constraints on subduction geodynamics from seismic anisotropy. *Reviews of Geophysics*, *51*(1), 76–112. https://doi.org/10.1002/rog.20008

Lu, C., Grand, S. P., Lai, H., & Garnero, E. J. (2019). TX2019slab: A new *P* and *S* tomography model incorporating subducting slabs. *Journal of Geophysical Research: Solid Earth*, *124*(11), 11549–11567. https://doi.org/10.1029/2019JB017448

McNamara, A. K., & Zhong, S. (2004). Thermochemical structures within a spherical mantle: Superplumes or piles? *Journal of Geophysical Research*, *109*(B7), 2003JB002847. https://doi.org/10.1029/2003JB002847

Moresi, L., Zhong, S., Han, L., Conrad, C., Tan, E., Gurnis, M., et al. (2014). CitcomS v3.3.1 (v3.3.1). [Software]. *Zenodo*. https://doi.org/10.5281/zenodo.7271920

Obayashi, M., Yoshimitsu, J., Nolet, G., Fukao, Y., Shiobara, H., Sugioka, H., et al. (2013). Finite frequency whole mantle *P* wave tomography: Improvement of subducted slab images. *Geophysical Research Letters*, *40*(21), 5652–5657. https://doi.org/10.1002/2013GL057401

Palmiotto, C., Ficini, E., Loreto, M. F., Muccini, F., & Cuffaro, M. (2022). Back-Arc spreading centers and superfast subduction: The case of the northern Lau basin (SW Pacific ocean). *Geosciences*, *12*(2), 50. https://doi.org/10.3390/geosciences12020050

Peng, D. (2024). Parameters and results of 2D Tonga subduction models. [Dataset]. *Zenodo*. https://doi.org/10.5281/zenodo.12626942

Peng, D., & Liu, L. (2023). Importance of global spherical geometry for studying slab dynamics and evolution in models with data assimilation. *Earth-Science Reviews*, *241*, 104414. https://doi.org/10.1016/j.earscirev.2023.104414

Peng, D., Liu, L., Hu, J., Li, S., & Liu, Y. (2021). Formation of East Asian stagnant slabs due to a pressure-driven cenozoic mantle wind following mesozoic subduction. *Geophysical Research Letters*, *48*(18), e2021GL094638. https://doi.org/10.1029/2021GL094638

Pokorný, J., Čížková, H., Bina, C. R., & Van Den Berg, A. (2023). 2D stress rotation in the Tonga subduction region. *Earth and Planetary Science Letters*, *621*, 118379. https://doi.org/10.1016/j.epsl.2023.118379

Price, A. A., Jackson, M. G., Blichert-Toft, J., Hall, P. S., Sinton, J. M., Kurz, M. D., & Blusztajn, J. (2014). Evidence for a broadly distributed Samoan-plume signature in the northern Lau and north Fiji basins: Lau and north Fiji basins. *Geochemistry, Geophysics, Geosystems*, *15*(4), 986–1008. https://doi.org/10.1002/2013GC005061

Pysklywec, R. N., Mitrovica, J. X., & Ishii, M. (2003). Mantle avalanche as a driving force for tectonic reorganization in the southwest Pacific. *Earth and Planetary Science Letters*, *209*(1–2), 29–38. https://doi.org/10.1016/S0012-821X(03)00073-6

Richards, S., Holm, R., & Barber, G. (2011). When slabs collide: A tectonic assessment of deep earthquakes in the Tonga-Vanuatu region. *Geology*, *39*(8), 787–790. https://doi.org/10.1130/G31937.1

Schellart, W. P., Freeman, J., Stegman, D. R., Moresi, L., & May, D. (2007). Evolution and diversity of subduction zones controlled by slab width. *Nature*, *446*(7133), 308–311. https://doi.org/10.1038/nature05615

Schellart, W. P., Stegman, D. R., & Freeman, J. (2008). Global trench migration velocities and slab migration induced upper mantle volume fluxes: Constraints to find an Earth reference frame based on minimizing viscous dissipation. *Earth-Science Reviews*, *88*(1–2), 118–144. https://doi.org/10.1016/j.earscirev.2008.01.005

Schellart, W. P., & Strak, V. (2021). Geodynamic models of short-lived, long-lived and periodic flat slab subduction. *Geophysical Journal International*, *226*(3), 1517–1541. https://doi.org/10.1093/gji/ggab126

Schmeling, H., Babeyko, A. Y., Enns, A., Faccenna, C., Funiciello, F., Gerya, T., et al. (2008). A benchmark comparison of spontaneous subduction models—Towards a free surface. *Physics of the Earth and Planetary Interiors*, *171*(1–4), 198–223. https://doi.org/10.1016/j.pepi.2008.06.028

Stadler, G., Gurnis, M., Burstedde, C., Wilcox, L. C., Alisic, L., & Ghattas, O. (2010). The dynamics of plate tectonics and mantle flow: From local to global scales. *Science*, *329*(5995), 1033–1038. https://doi.org/10.1126/science.1191223

Stegman, D. R., Freeman, J., Schellart, W. P., Moresi, L., & May, D. (2006). Influence of trench width on subduction hinge retreat rates in 3-D models of slab rollback. *Geochemistry, Geophysics, Geosystems*, *7*(3), 2005GC001056. https://doi.org/10.1029/2005GC001056

Syracuse, E. M., Van Keken, P. E., & Abers, G. A. (2010). The global range of subduction zone thermal models. *Physics of the Earth and Planetary Interiors*, *183*(1–2), 73–90. https://doi.org/10.1016/j.pepi.2010.02.004

Tackley, P. J., Stevenson, D. J., Glatzmaier, G. A., & Schubert, G. (1993). Effects of an endothermic phase transition at 670 km depth in a spherical model of convection in the Earth's mantle. *Nature*, *361*(6414), 699–704. https://doi.org/10.1038/361699a0

Tan, E., & Gurnis, M. (2007). Compressible thermochemical convection and application to lower mantle structures. *Journal of Geophysical Research*, *112*(B6), 2006JB004505. https://doi.org/10.1029/2006JB004505

Van Keken, P. E., Hacker, B. R., Syracuse, E. M., & Abers, G. A. (2011). Subduction factory: 4. Depth-Dependent flux of H_2O from subducting slabs worldwide. *Journal of Geophysical Research*, *116*(B1), B01401. https://doi.org/10.1029/2010JB007922

Wallace, L. M., McCaffrey, R., Beavan, J., & Ellis, S. (2005). Rapid microplate rotations and backarc rifting at the transition between collision and subduction. *Geology*, *33*(11), 857. https://doi.org/10.1130/G21834.1

Yu, Z., Zhao, D., & Li, J. (2022). Structure and dynamics of the Tonga subduction zone: New insight from P-wave anisotropic tomography. *Earth and Planetary Science Letters*, *598*, 117844. https://doi.org/10.1016/j.epsl.2022.117844

Zhong, S., Zuber, M. T., Moresi, L., & Gurnis, M. (2000). Role of temperature-dependent viscosity and surface plates in spherical shell models of mantle convection. *Journal of Geophysical Research*, *105*(B5), 11063–11082. https://doi.org/10.1029/2000JB900003